CHEMISTRY
A EUROPEAN JOURNAL

FULL PAPER

DOI: 10.1002/chem.201300421

Shape-Persistent (Pt-salphen)$_2$ Phosphorescent Coordination Frameworks: Structural Insights and Selective Perturbations

Zhengqing Guo, Shek-Man Yiu, and Michael C. W. Chan*[a]

Abstract: The development of molecular frameworks derived from binuclear platinum(II) aromatic Schiff base (salphen) complexes and their supramolecular chemistry have been undertaken. A series of axially rotating (Pt-salphen)$_2$ luminophores, tethered in a cofacial manner by a rigid linker (xanthene, **1**; dibenzofuran, **2**; biphenylene, **3**), was synthesized in which the O-(salphen) groups are potentially amenable for guest-binding. The molecular structures of **1** and **3** have been determined by X-ray crystallography, revealing intra- and intermolecular π-stacking interactions, as well as contrasting *syn* (**1**) and *anti* (**3**) configurations, for the (Pt-salphen)$_2$ moiety. All complexes are luminescent in solution at room temperature. Their photophysical and solvatochromic properties have been examined, and the emissions are assigned to mixed triplet O(p)/Pt(d)→π*(diimine) excited states. The red-shifted fluid emissions and lower quantum yields of **1** and **3**, relative to **2**, are ascribed to enhanced intramolecular π-stacking interactions. Photophysical changes and selective responses to metal ions (particularly Pb^{2+}) have been investigated by using various spectroscopic methods and DFT calculations, and through comparative studies with control complexes. A plausible binding mechanism is proposed based on occupation of the O(salphen)-binding cavity, which induces perturbation of intramolecular π–π interactions, and hence the self-quenching and emission properties, of the (Pt-salphen)$_2$ unit.

Keywords: luminescence · pi interactions · platinum · sensors · supramolecular chemistry

Introduction

The design and development of new functional molecular architectures is a core motivation in coordination and supramolecular chemistry.[1] Multidentate Schiff bases have been prominent in this regard,[2] and considerable efforts have been made to utilize these diverse building blocks in the construction of macrocycles[3] and metalated host molecules,[4] and to study their ion binding and transport properties[5] as well as aggregation and self-assembly[6] into supramolecular entities and nanostructures.[7,8] In recent years, the guest-binding abilities of multinuclear chiral hosts[9] and new transformations mediated by cooperative and biomimetic catalysts[10,11] have also been highlighted.

In the context of this work, the photophysical[12] and electronic[13] characteristics (and materials applications[14] and catalytic role[15]) of bis(metal-Schiff base) complexes have been investigated, and several of these systems have exploited the inherently rigid, planar nature of π-systems. More generally, design strategies evolved from molecular phenomena such as rigidification[16] and restricted rotation/conformation[17] in crowded aromatic architectures have been explored in search of desirable electronic,[18] catalytic[19] and recognition properties.[20] Although attention has been focused on organic hosts and fluorescent versions have been developed,[21] it is evident that transition-metal-based systems can engender advantages such as tunable, well-defined coordination geometries, and visible-light reporting. The related development of molecular tweezers,[22] clips, grippers, and related π-stacked host systems exhibiting interesting recognition, electronic and chiroptical characteristics have been described.[23]

We initiated a program to develop phosphorescent molecular hosts and assemblies, based on a modular design approach encompassing coordinatively unsaturated transition-metal-(π-organic) phosphorescent units (thus enabling axial substrate-binding interactions and signaling without interference from organic/background fluorescence) and a rigid, robust, and readily derivatizable supporting framework (that would link components and maintain structural integrity), with the aim of engendering molecular topologies with unusual photophysical and sensing properties. New classes of shape-persistent mono-,[24] bi-[25] and polynuclear[26] Pt^{II} coordination frameworks and materials, bearing integrated features that allow the reporting of molecular-level perturbations and events, have been developed. Our underlying objective is to devise new strategies to modulate, control, and signal the molecular motion in these systems, paving the way towards new functionalities and the realization of luminescent machines.

We are currently focused on creating congested molecular scaffolds derived from platinum(II) luminophores supported by aromatic Schiff bases. The incorporation of phosphores-

---

[a] Dr. Z. Guo, Dr. S.-M. Yiu, Dr. M. C. W. Chan
Department of Biology and Chemistry, City University of Hong Kong
Tat Chee Avenue, Kowloon, Hong Kong (P.R. China)
E-mail: mcwchan@cityu.edu.hk

Supporting information for this article is available on the WWW under http://dx.doi.org/10.1002/chem.201300421.

cent metal-organic moieties such as Pt-salphen (H_2-salphen = *N,N'*-bis(salicylidene)-1,2-phenylenediamine) into supramolecular architectures can confer beneficial properties: 1) compared with d^6 octahedral $Ru(bpy)_3^{2+}$ luminophores, which exhibit sphere-like coordination, the "open" geometry of square planar d^8 Pt^{II} can afford excited states that are sensitive to the micro-environment;[27] 2) diverse photophysical characteristics and high quantum efficiencies under ambient conditions have been reported;[28,29] 3) modification and functionalization of the ligand structure is well-established. We recently described new phosphorescent $(Pt\text{-salphen})_2$ frameworks and their colorimetric and luminescent responses to metal ions.[30] The two Pt-salphen fragments are tethered cofacially to a rigid backbone to create a potential O_4-binding cavity, whereas correlated axial rotation would afford intramolecular interactions. Herein, we have elaborated upon our previous work by employing different rigid backbones (**1**–**3**), which would modulate the separation and angle, and thus the extent of interaction, between the two Pt-salphen moieties in these complexes, and probed the impact of this upon photophysical properties and binding/sensing behavior. Intriguingly, the occupation of the $(Pt\text{-salphen})_2$ cavity could result in the disruption of π–π (and possibly Pt···Pt) interactions, which would be signaled by the intrinsically responsive Pt^{II} luminophores. The colorimetric and phosphorescent responses of these host structures upon addition of metal ions have been investigated. Control complexes (**4** and **5**) have been studied in concert, and a variety of spectroscopic techniques plus DFT calculations have been employed, to rationalize the photophysical changes and provide insight into the binding mechanism. These observations may be of relevance to luminescent host complexes displaying intramolecular interactions that undergo photophysical changes in response to external stimuli.

Results and Discussion

Preparation of platinum(II) Schiff base complexes: A modular approach was employed for the synthesis of the binuclear platinum(II) Schiff base complexes **1**–**3** (see the Supporting Information for details). The important brominated salphen-Pt^{II} precursor **L1** was obtained by treatment of the corresponding Schiff base (**C1**) with K_2PtCl_4 in the presence of K_2CO_3 in DMSO at 75 °C. Regarding the rigid backbones, the substituted xanthene and dibenzofuran precursors are commercially available, but preparation of the biphenylene backbone required several steps and modification of literature procedures. Bromination of *p-tert*-butylaniline afforded the dibromoaniline **C2**, which was subsequently diazotized in sulfuric and glacial acetic acids with $NaNO_2$, then treated with iodine, to form **C3**. An Ullmann coupling reaction was employed in the synthesis of the key intermediate **C4**:[31] compound **C3** was converted into the desired aryllithium intermediate by means of halogen/metal permutation, followed by reaction with stoichiometric amounts of copper(II) bromide and nitrobenzene, then reductive elimination, to afford the biaryl compound **C4**. Finally, a modified Ullmann cyclization by using copper(II)-mediated oxidative coupling yielded the dibromobiphenylene **C5**.[32]

Functionalization of the rigid backbones was achieved by activation of two bromide atoms through halogen-lithium exchange with *n*BuLi. The intermediate was subsequently reacted with 2 equiv of $B(OMe)_3$ and hydrolyzed into the bisboronic acids **B1–B3**. Treatment of the respective bisboronic acids with 2 equiv of **L1** in the presence of $[Pd(PPh_3)_4]$ and K_2CO_3 in degassed DMF solution at 75 °C afforded the desired binuclear complexes **1**–**3** as dark-red solids (Scheme 1). The control complexes **4** and **5** were prepared

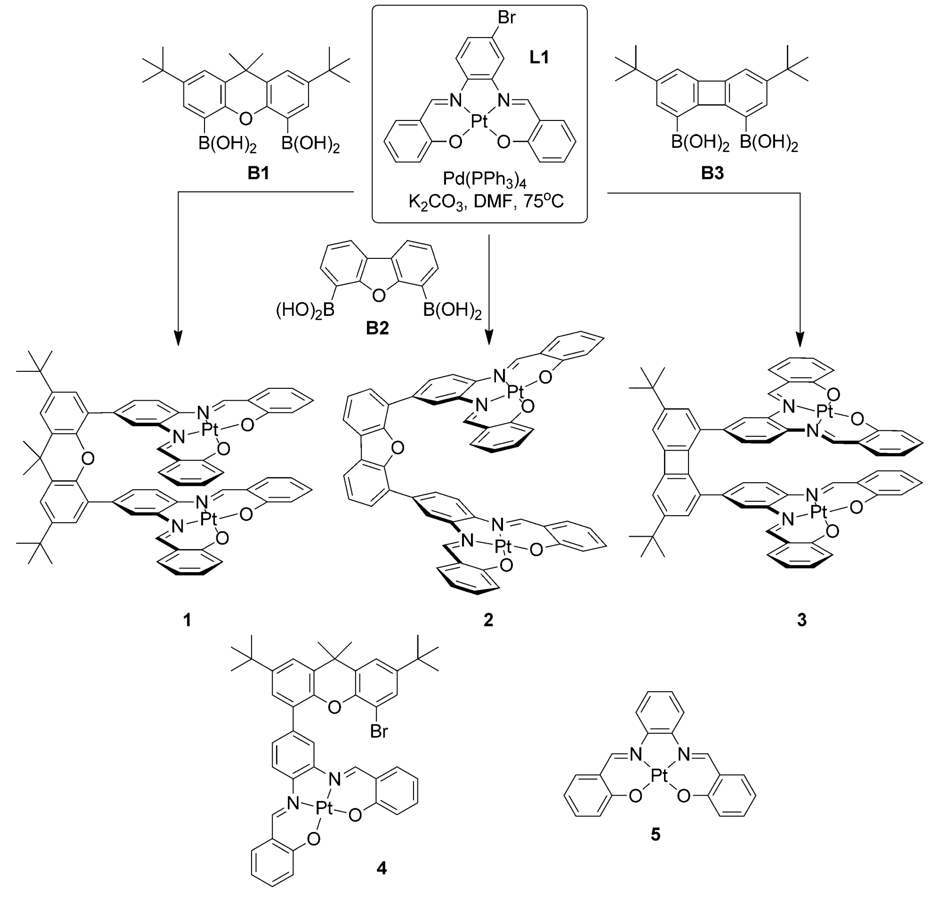

Scheme 1. Synthesis of **1**–**3**, and structures of control complexes **4** and **5**.

similarly or according to a literature method.[28a] All Pt^{II} complexes were characterized by NMR spectroscopy, ESI-MS, and elemental analysis. In the ESI mass spectra, parent clusters with m/z values that closely match the respective theoretical isotopic patterns were observed (Figures S1–S3 in the Supporting Information).

Crystal structures of (Pt-salphen)$_2$ complexes: Single crystals of **1** and **3** were obtained by slow evaporation of ethyl acetate solutions, and structural determinations were performed by X-ray crystallography (Figures 1 and 2, respectively, and the Supporting Information).[33] For the xanthene-based complex **1**, the square planar geometry around the two platinum atoms are generally unremarkable, and each Pt-salphen unit is planar with negligible deviation of the aryl rings. The mean Pt−N and Pt−O distances in **1** are 1.963 and 1.997 Å, respectively, resembling those previously reported for Pt^{II} Schiff base complexes.[14,28,29] The two Pt-salphen moieties are bridged by the xanthene backbone in a *syn* cofacial fashion, with dihedral angles of around 43° to the xanthene plane. The intramolecular Pt(1)···Pt(2) distance of 5.012(2) Å (Figure S4 in the Supporting Information) signify the absence of Pt···Pt interactions, although the shorter intermolecular Pt(2)···Pt(2*) separation of 3.431(2) Å may be interpreted as a weak interaction. Importantly, the intra- and intermolecular interplanar separations (defined as mean separation between Pt and adjacent N_2O_2 plane) of 3.22 and 3.25 Å, respectively, indicate the existence of π–π interactions between the coplanar Pt-salphen moieties (Figure 1).

The geometry of both platinum atoms in the biphenylene-based **3** (Figure 2) are also square planar. Compared with **1**, distortion of the aryl rings from the Pt(N_2O_2) planes, especially for Pt(1), is more discernible but remains slight. The mean Pt−N (1.962 Å) and Pt−O (1.994 Å) distances in **3** are comparable to **1** and related complexes. In contrast to **1**, the two Pt-salphen moieties are linked to the biphenylene unit in an *anti* cofacial manner, and the dihedral angles to the biphenylene plane are smaller (ca. 36°). This, together with the narrower biphenylene spacer, gives rise to a shorter Pt(1)···Pt(2) distance of 3.359(2) Å, which constitutes a weak intramolecular Pt···Pt interaction[14,23b,27a,34] (Figure S5 in the Supporting Information). The intramolecular interplanar separation of 3.36 Å between the Pt-salphen moieties in

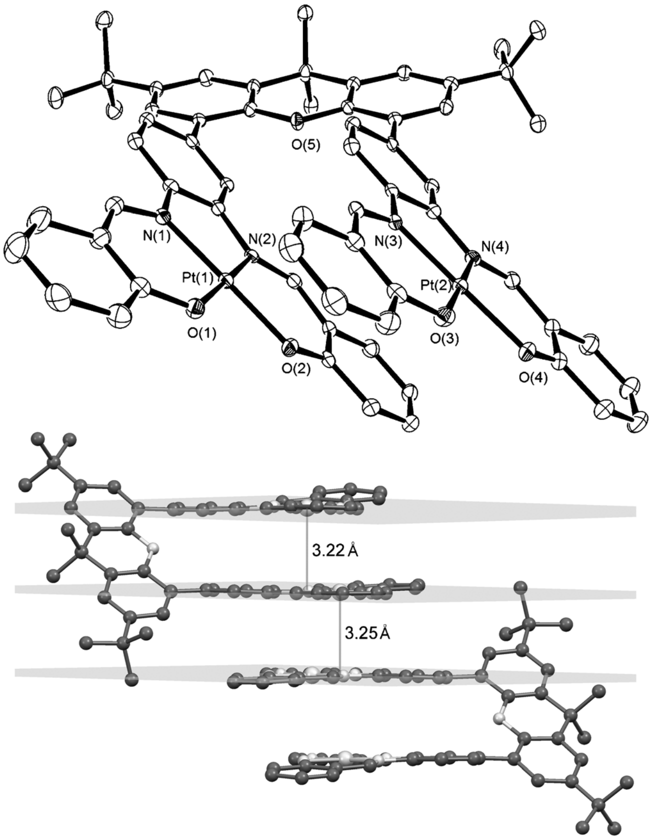

Figure 1. Perspective view (top; 50% probability ellipsoids) and packing diagram (bottom; showing intra- and intermolecular π–π separations) of **1**. Selected bond lengths [Å] and angles [°]: Pt(1)−N(1) 1.962(4), Pt(1)−N(2) 1.967(3), Pt(1)−O(1) 1.997(3), Pt(1)−O(2) 1.991(3), Pt(2)−N(3) 1.963(4), Pt(2)−N(4) 1.960(4), Pt(2)−O(3) 2.000(3), Pt(2)−O(4) 1.998(3), Pt(1)···Pt(2) 5.012(2), N(1)-Pt(1)-N(2) 83.8(1), N(1)-Pt(1)-O(1) 95.2(1), N(1)-Pt(1)-O(2) 178.6(1), O(1)-Pt(1)-O(2) 85.5(1).

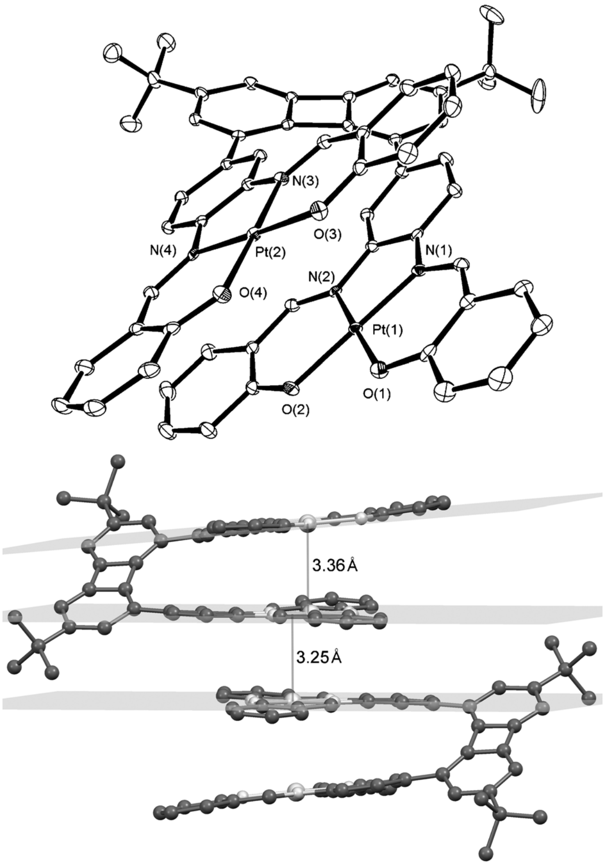

Figure 2. Perspective view (top; 50% probability ellipsoids) and packing diagram (bottom; showing intra- and intermolecular π–π separations) of **3**. Selected bond lengths [Å] and angles [°]: Pt(1)−N(1) 1.955(4), Pt(1)−N(2) 1.967(3), Pt(1)−O(1) 1.996(3), Pt(1)−O(2) 1.989(3), Pt(2)−N(3) 1.972(3), Pt(2)−N(4) 1.955(4), Pt(2)−O(3) 1.995(3), Pt(2)−O(4) 1.995(3), Pt(1)···Pt(2) 3.359(2), N(1)-Pt(1)-N(2) 83.5(1), N(1)-Pt(1)-O(1) 95.4(1), N(1)-Pt(1)-O(2) 178.7(1), O(1)-Pt(1)-O(2) 85.4(1).

3 is slightly larger than that in **1** (3.22 Å), and the adjacent N_2O_2 planes are not coplanar (angle = 4.9°). Although this suggests less favorable π–π interaction in the solid state for the *anti* cofacial Pt-salphen units in **3**, crystal packing effects should be considered. The intermolecular interplanar separation (3.25 Å) and Pt(2)···Pt(2*) distance (3.336(2) Å) in **3** are comparable to those in **1**, and indicate the possibility of intermolecular π–π and Pt···Pt interactions in the solid state. These structural features may be useful for rationalizing the luminescent properties of these complexes, whereas the contrasting *syn* and *anti* (Pt-salphen)$_2$ configurations in **1** and **3**, respectively, is envisaged to impact upon binding characteristics. A detailed comparison of photophysical properties is presented in the next section.

Absorption and emission spectroscopy: The photophysical properties of complexes **1**–**4** have been examined by UV/Vis absorption and emission spectroscopy (Table 1; the photophysical data for **5** was reported previously[28c]). The UV/Vis absorption spectra of the binuclear complexes **1**–**3** in CH_2Cl_2 (Figure S6 in the Supporting Information) contain bands at <390 nm ($\varepsilon > 2.0\times10^4$ dm^{3}mol^{-1}cm^{-1}) that closely resemble the structured nature and extinction coefficients of the corresponding non-metalated ligands. In addition, less intense absorptions are observed in the visible region at λ_{max} 454–552 nm ($\varepsilon = (6\text{–}10)\times10^3$ dm^{3}mol^{-1}cm^{-1}) that are absent from the ligand precursors. As described in previous spectroscopic studies of phenyl-substituted analogues,[28,35] the bands at <390 nm are ascribed to intraligand $^1(\pi\pi^*)$ transitions, whereas the low-energy absorptions at λ_{max} 454–552 nm are assigned as O(p)/Pt(d)→π*(diimine) charge-transfer transitions.

Complexes **1**–**3** display structureless red emission (λ_{max} 630–640 nm) in CH_2Cl_2 at 298 K, with long emission lifetimes indicating phosphorescence. The lower Φ_{em} values and broader emission band-shape for **1** and **3** may be attributed to greater intramolecular π–π interaction between the cofacially tethered Pt-salphen moieties, which is known to cause self-quenching.[17d,25,36] To characterize the photophysical nature of these binuclear complexes in detail, the time-resolved difference absorption spectra of **1** in degassed CH_3CN were recorded after 355 nm nanosecond laser excitation (Figure S7 in the Supporting Information). The prominent features in the transient absorption (TA) spectra are photo-bleaching at around 650 nm and strong absorptions in the 400–600 nm region. The TA lifetime (0.19 μs) is in good agreement with the emission lifetime in CH_3CN (0.17 μs), which is in accordance with the absorption originating from the emissive excited state.

To provide information and insight for sensing studies, a comparison of the emission energies and band-shapes for complexes **1**–**5** in CH_2Cl_2/CH_3CN (1/1) is shown in Figure 3. The fluid emissions are assigned to mixed triplet O(p)/Pt(d)→π*(diimine) excited states, which are reported to undergo blue-shifts in more polar solvents due to the polar character of the electron-rich oxygen donor in the ground state.[28,35] This is indeed observed for **2** (from λ_{max} 637 (in

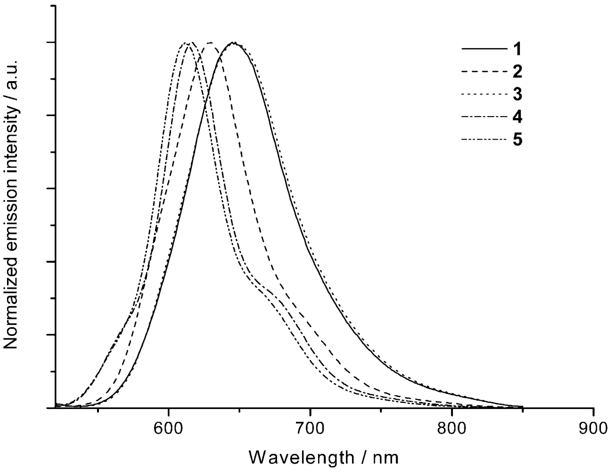

Figure 3. Normalized emission spectra of **1**–**5** (10^{-5} M) in CH_2Cl_2/CH_3CN (1:1) at 298 K.

Table 1. Photophysical data for **1**–**4**.

			Fluid: λ_{max} [nm] (τ [μs]); Φ		Solid: λ_{max} [nm] (τ [μs])	
Cpd	λ_{max} [nm] (ε [dm^3 mol^{-1}cm^{-1}])	λ_{ex} [nm]	298 K	77 K[c]	298 K	77 K
1	259 (53730), 303 (27590), 325 (31370), 366 (36570), 472 (8410), 535 (8970), 547 (8900)[a]	546	635 (0.20); 0.007[a] 645[b]	650 (max; 7.0), 617, 705	668 (0.040)	679 (0.37)
2	260 (35510), 329 (26620), 371 (30120), 388 (29500), 454 (5950), 475 (6960), 537 (7220), 552 (7370)[a]	555	635 (2.73); 0.080[a] 630[b]	613 (max; 8.2), 647, 748	659 (0.014)	665 (max; 1.06), 730 (0.75)
3	257 (54180), 326 (30250), 374 (32480), 477 (7390), 534 (7750), 553 (7780)[a]	520	642 (0.16); 0.009[a] 647[b]	609 (max; 14.7), 648, 710	680 (0.064)	677 (max; 0.37), 742 (0.28)
4	255 (24320), 293 (9860), 308 (10510), 318 (10780), 342 (11240), 361 (17900), 377 (18690), 429 (1890), 457 (3870), 526 (4620)[d]	501	615 (max; 3.92), 667; 0.061[d] 617 (max), 670[b]	605 (max; 11.5), 663	660 (0.188)	657 (4.28)

[a] In CH_2Cl_2. [b] In CH_2Cl_2/CH_3CN (1:1). [c] In 2-Me-THF. [d] In CH_3CN.

toluene) to 635 (CH_2Cl_2) and 626 nm (CH_3CN)) and **5** (from λ_{max} 629 (in toluene) to 617 (CH_2Cl_2) and 612 nm (CH_3CN)), but not **1** (from λ_{max} 661 (in toluene) to 635 (CH_2Cl_2) and 639 nm (CH_3CN)) and **3** (from λ_{max} 672 (in toluene) to 642 (CH_2Cl_2) and 648 nm (CH_3CN); Figure S8 in the Supporting Information). Furthermore, the conventional negative solvatochromic emissions of **2** and **5** are more structured than the broader emissions of **1** and **3**. It is therefore postulated that intramolecular π–π interactions between Pt-salphen moieties in **1** and **3** may be enhanced in CH_3CN as well as toluene, giving rise to the red-shifted emissions. In CH_2Cl_2/CH_3CN (1/1), the uncharacteristic red-shifted emissions for **1** and **3**, which are concentration-independent down to 10^{-7} M (thus discounting aggregation), are attributed to intramolecular π–π interactions as observed in the crystal structures (i.e., offset interplanar π-contacts within the (Pt-salphen)$_2$ moiety). Such π-stacked interactions are prevalent in **1** and **3**, resulting in broad, unstructured emissions at λ_{max} 648 nm, weaker in dibenzofuran-linked **2** to give a blue-shifted emission with narrower band-shape at λ_{max} 628 nm (resulting in a higher Φ_{em} for **2** (due to decreased self-quenching) compared with **1** and **3**), and absent in control complexes **4** and **5** to afford further blue-shifted and structured emissions at around λ_{max} 610 nm, which is typical for non-aggregated Pt-salphen monomer species.

The solid-state (298 and 77 K) and glassy (77 K) emissions of **1**–**5** have also been examined (Figure S9 and S10 in the Supporting Information). In the solid state, compounds **1**–**3** display structureless low-energy emissions ($\lambda_{max} > 658$ nm) at 298 K. The binuclear complex **3** displays the most red-shifted solid emission at λ_{max} 680 nm, which is tentatively attributed to intra- as well as intermolecular π–π and Pt⋅⋅⋅Pt interactions, corresponding to those observed in the crystal structure. Whereas the parent mononuclear complex **5** displays a structured solid-state emission at λ_{max} 620 nm at 298 K, the control derivative **4** exhibits a structureless red-shifted emission at λ_{max} 660 nm, resembling that of **2**. Evidently, the intermolecular π-stacking interactions and packing effects for **1**–**5** in the solid state are different. The solid-state emissions at 77 K are slightly more structured, but similar results are observed. The 77 K glassy emission for **1** is red-shifted (λ_{max} 650 nm), but the remaining complexes display highly structured emissions at λ_{max} 600–613 nm with vibronic progressions of around 1300 cm^{-1}. Such vibronic structure is emblematic of $^3\pi\pi^*$ excited states, but the solid-state and glassy emissions in this work are excessively red-shifted for this assignment and thus ascribed to mixed triplet O(p)/Pt(d)→π*-(diimine) excited states.

Photophysical responses to metal ions: perturbation of π-stacked interactions: The binding characteristics of **1** has been investigated by using UV/Vis and emission spectroscopy with various mono- and divalent metal ions (as perchlorate salts) in CH_3CN. With 1.0 equiv of M^{n+} ions, the 639 nm emission was converted into a structured band at λ_{max} 605 nm for the Pb^{2+} ion only, and further addition yielded no change. For Cu^{2+} and Hg^{2+} ions, the emission was steadily quenched, whereas for Mg^{2+}, Ca^{2+}, Zn^{2+}, Cd^{2+}, and all monovalent metals ions, there were minimal or no responses (Figure S11 in the Supporting Information). Competition experiments signifying a ratiometric phosphorescent response and selectivity for Pb^{2+} have been conducted (Figure 4), in which the emission intensity of **1** (3.5×10^{-5} M in CH_3CN) were monitored at both 639 and 605 nm in the presence of the metal ions (1.0 equiv). A clear colorimetric response was also detected for **1** with 1.0 equiv of Pb^{2+}, and to some extent Cu^{2+} and Hg^{2+}, corresponding to the incremental decrease of the 535 nm absorption with increasing [M^{2+}] (Figure S11 in the Supporting Information). Analogous experiments for complex **3** with various metal ions were performed (Figure S12 in the Supporting Information). Like **1**, there were minimal or no responses for Mg^{2+}, Ca^{2+}, Zn^{2+}, Cd^{2+}, and all monovalent metals ions, whereas quenching was observed for Cu^{2+} and Hg^{2+} ions. In contrast to **1**, a quenched emission that was nevertheless blue-shifted was recorded for **3** upon addition of Pb^{2+} ions.

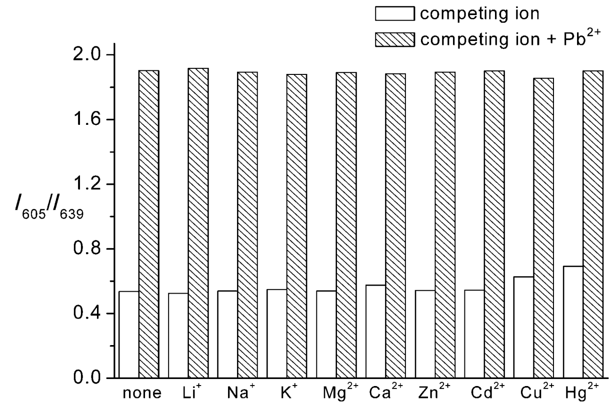

Figure 4. Competition experiments showing ratiometric phosphorescent response and selectivity by **1** for Pb^{2+} ions. $Pb(ClO_4)_2$ (1.0 equiv) was added after solutions of **1** in CH_3CN (3.5×10^{-5} mol L^{-1}) had been incubated with 1.0 equiv of metal ions (λ_{ex} 501 nm).

Quantitative titrations have been performed to probe the photophysical responses in CH_3CN. The UV/Vis spectral changes for **1** became saturated after addition of 1.0 equiv of Pb^{2+} ions and revealed a well-defined isosbestic point at 501 nm (Figure S13 in the Supporting Information), which was used as the emission λ_{ex}. In the emission titration, incremental changes were detected for up to 1.0 equiv of Pb^{2+} ions, and saturation occurred thereafter (Figure 5, top). The broad red emission at λ_{max} 639 nm was blue-shifted and transformed into a structured emission at λ_{max} 605 nm (termed "monomer-like" since it closely resembles the energy and band-shape of the respective emission for **4** and **5**). In addition, the aerated emission lifetime ($\lambda_{639} = 0.07$ μs) became noticeably longer after the addition of Pb^{2+} ions ($\lambda_{605} = 0.33$ μs). It is of interest to note that literature reports of phosphorescent hosts that are capable of sensing Pb^{2+} ions remain sparse.[37] The reversibility of the photophysical response of **1** to Pb^{2+} ions was demonstrated (Figure S14 in

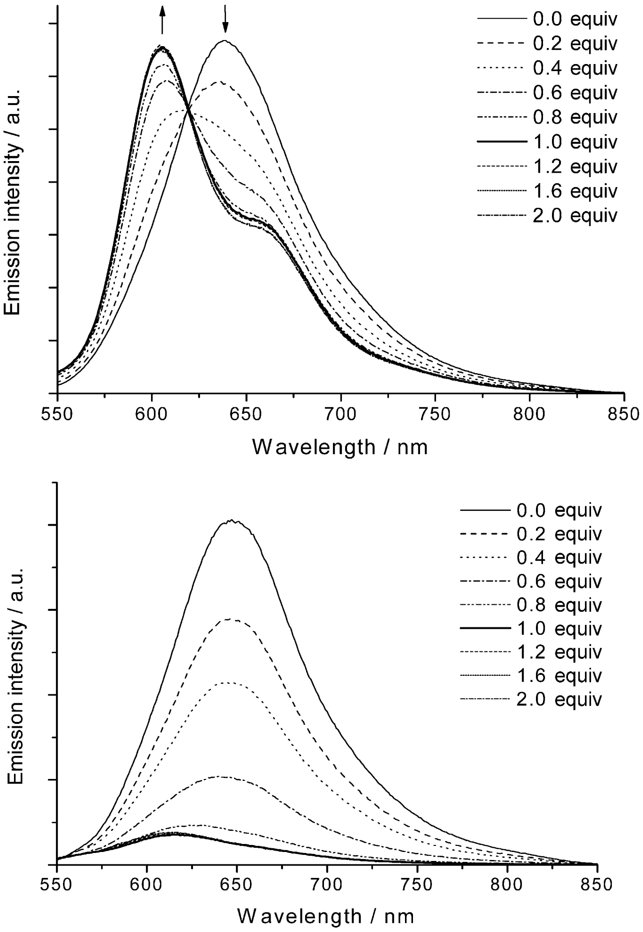

Figure 5. Quantitative emission titrations (λ_{ex} 501 nm) for **1** (top; 5×10^{-5} M) and **3** (bottom; 2.5×10^{-5} M) in CH_3CN upon addition of Pb^{2+} ions.

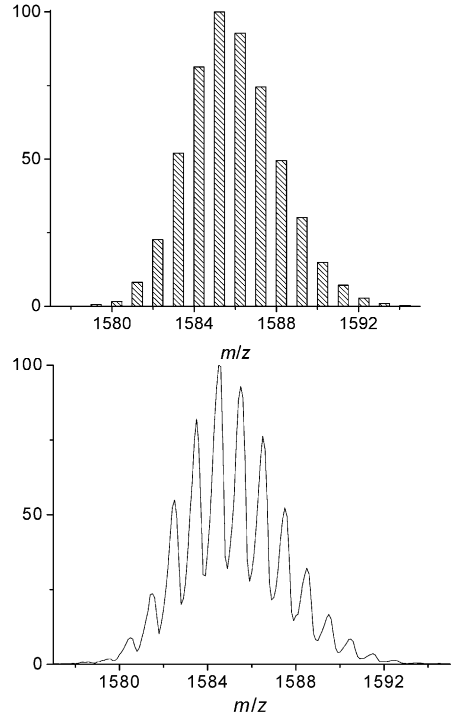

Figure 6. ESI-MS of $[\mathbf{3}+Pb+ClO_4]^+$ in CH_3CN using zero declustering potential (top: calculated isotopic distribution).

the Supporting Information).[38] Quantitative emission titrations have also been performed for **3** in CH_3CN (Figure 5, bottom). Incremental changes were detected upon addition of up to 1.0 equiv of Pb^{2+} ions, after which saturation occurred. In stark contrast to **1**, the broad red emission at λ_{max} 648 nm was gradually quenched and blue-shifted to λ_{max} 616 nm.

^{1}H NMR studies have been conducted for **1** in the presence of Pb^{2+} ions (Figure S15 in the Supporting Information). The ^{1}H NMR shift differences between each side of the non-symmetric salphen fragment became greater, indicative of increased rigidity. The binding process for **1** was investigated by using ESI mass spectrometry (Figure S16 in the Supporting Information). The major signal in the ESI mass spectrum of **1** with 1.0 equiv of Pb^{2+} in CH_3CN, using zero declustering potential, is a cluster at *m*/*z* 1643.2, which displays excellent agreement with the calculated isotopic pattern for the $[\mathbf{1}+Pb+ClO_4]^+$ species with 1 amu separation between peaks. In the analogous ESI-MS of **3** with Pb^{2+} (1.0 equiv), the dominant signal is a cluster at *m*/*z* 1584.5 (1 amu separations) corresponding closely to $[\mathbf{3}+Pb+ClO_4]^+$ (Figure 6).[39] These results imply that when bound by **1** or **3**, the Pb^{2+} ion can remain coordinated by perchlorate, possibly in a bidentate mode like that reported by Carbonaro et al.[40] in the crystal structure of $[\{Ni(salen)\}_2{\cdot}Ba(ClO_4)_2(thf)]$, featuring two chelating perchlorate groups at Ba^{2+} (plus O_4-coordination by two mononuclear Ni-salen moieties), and by Lalinde et al.[41] in the crystal structure of $(NBu_4)[\{Pt(bzq)(C{\equiv}CC_6H_4\text{-}4\text{-}CF_3)_2\}_2{\cdot}Pb(ClO_4)]$ (bzq = 7,8-benzoquinoline), in which the Pb^{2+} ion is coordinated by a bidentate perchlorate group, as well as four acetylide moieties of two $[Pt(bzq)(C{\equiv}CAr)_2]$ units in a $[\eta^1(C{\equiv}CAr)]_4$ binding mode.

To elucidate the mechanism for Pb^{2+}-binding by **1** and **3**, exhaustive attempts have been made to grow crystals suitable for structural determination by using a wide variety of solvents and mixtures thereof, numerous recrystallization methods, and different ratios of complex-to-Pb^{2+}, but these efforts have not succeeded. DFT calculations have been undertaken to investigate the structures of the $[\mathbf{1}+Pb+ClO_4]^+$ and $[\mathbf{3}+Pb+ClO_4]^+$ species observed by ESI-MS (Figure 7). Generally, the two energy-minimized calculated structures (each confirmed to be a minimum from vibrational frequency calculations) display many similarities: the Pb^{2+} ion resides close to the center of the O_4 cavity and is bound by a bidentate perchlorate group, the mean Pb–O(salphen) (**1**: 2.478 Å; **3**: 2.488 Å) and Pb–O(perchlorate) (**1**: 2.520; **3**: 2.516 Å) distances are comparable, and the Pb•••Pt distances (**1**: 3.260, 3.377; **3**: 3.289, 3.311 Å) are not dissimilar. However, while noting the contrasting *syn* and *anti* (Pt-salphen)$_2$ configurations in **1** and **3**, respectively, the mean separation between Pt and the adjacent N_2O_2 plane is signifi-

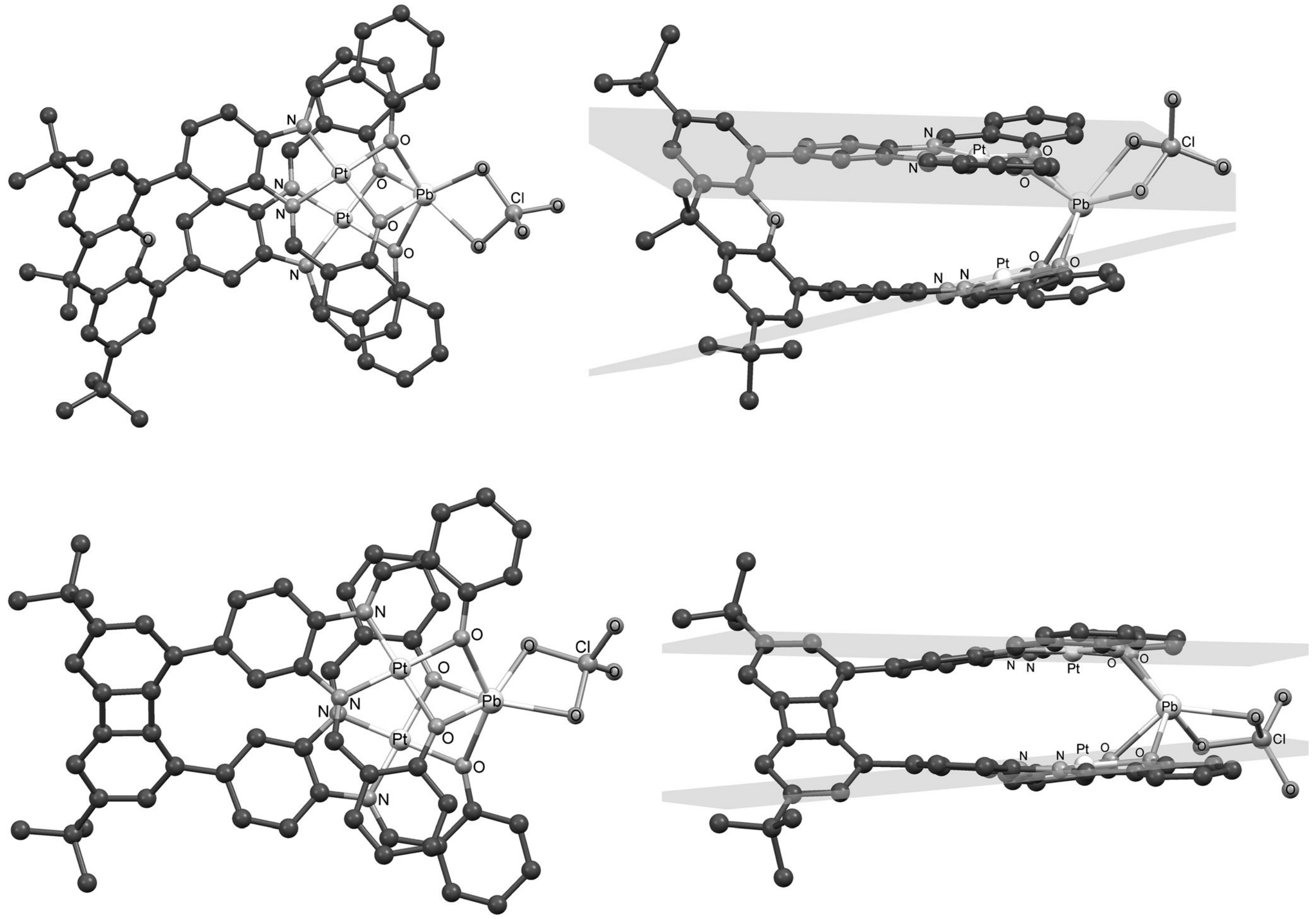

Figure 7. Energy-minimized calculated structures of $[\mathbf{1}+\mathrm{Pb}+\mathrm{ClO_4}]^+$ (top) and $[\mathbf{3}+\mathrm{Pb}+\mathrm{ClO_4}]^+$ (bottom): perspective view (left) and angle between N_2O_2 planes (right).

cantly greater in **1** (3.60 Å, c.f. 3.39 Å in **3**). Furthermore, the angle between the N_2O_2 planes is larger in **1** (18.2, c.f., 7.4° in **3**). By comparing these calculated structural parameters with the interplanar π–π separations in the crystal structures of **1** (3.22 Å; parallel) and **3** (3.36 Å; 4.9° between N_2O_2 planes), it is proposed that upon binding of Pb^{2+}, complex **1** may undergo conformational changes that separate the Pt-salphen moieties and disrupt the π–π interaction. In contrast, the structural impact of Pb^{2+} coordination upon the (Pt-salphen)$_2$ unit in **3** may be relatively small, and intramolecular π–π interactions would remain feasible. Notwithstanding the absence of solvent effects in the calculated structures, these differences may be helpful for explaining the contrasting emission responses to Pb^{2+} ions (see below).

Comparisons and general remarks: Further studies on the binuclear as well as control complexes have been undertaken to rationalize the observed spectral changes and possible binding mechanism. Quantitative experiments have been performed to investigate the emission quenching responses of **1** to Cu^{2+} and Hg^{2+} ions in CH_3CN (Figure S17 in the Supporting Information). For both Cu^{2+} and Hg^{2+}, the 639 nm emission of **1** was rapidly quenched but not shifted, and the resultant lifetime of **1** was observed to be independent of $[Cu^{2+}]$ or $[Hg^{2+}]$ ($\tau_o/\tau=1$, $\tau_o=0.07\,\mu s$), indicating static quenching processes. Furthermore, the absence of a blue-shift (or transformation to a "monomer-like" emission) signifies that the π-stacking within the (Pt-salphen)$_2$ unit in **1** is not disrupted by the Cu^{2+} (or Hg^{2+}) ions, and therefore suggests that the quenching (through metallophilic[42] or spin-orbit interactions) occurs outside the (Pt-salphen)$_2$ cavity. Upon addition of Pb^{2+} ions, the structured emissions of **4** and **5** in CH_3CN at around λ_{max} 610 nm was quenched but not shifted; this demonstrates that emission quenching is evidently the normal response of mononuclear Pt-salphen to Pb^{2+} ions, and tentatively implies that the binding of Pb^{2+} by **1** occurs inside the (Pt-salphen)$_2$ cavity.

The different backbones in **1**–**3** would modulate the nature and geometry of the (Pt-salphen)$_2$ cavity with regards to guest-binding, and hence their comparative emission responses to Pb^{2+} ions (1.0 equiv) have been investigated (Figure 8; CH_2Cl_2/CH_3CN (1:1) is used because **2** displays limited solubility in CH_3CN). For **2**, although a blue-shift to λ_{max} 605 nm was detected like **1**, the emission intensity was quenched to 80% of the original intensity (by peak area), which is in clear contrast to **1** (99% of original intensity;

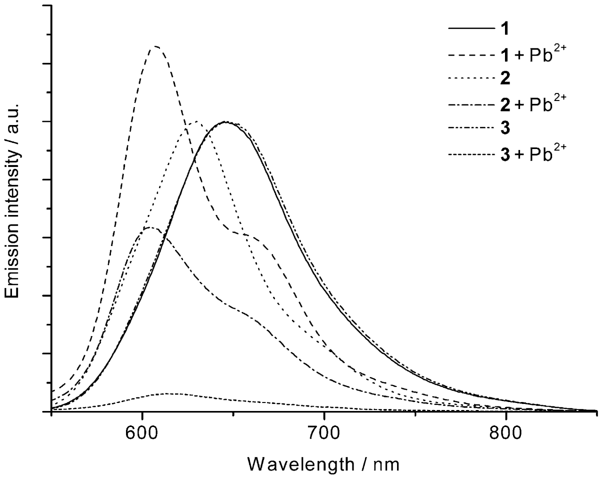

Figure 8. Emission spectra of **1**–**3** (normalized, 2×10^{-5} M, λ_{ex} 501 nm) in CH_2Cl_2/CH_3CN (1:1) showing relative changes upon addition of Pb^{2+} ions (1.0 equiv).

this blue-shifted emission band at λ_{max} 607 nm is also more structured) but comparable to **4** and **5** (86 and 90% of the respective original intensity). For **3**, the corresponding blue-shift to λ_{max} 616 nm is smaller than for **1**, and substantial emission quenching (9% of original intensity) was observed. The stoichiometry of Pb^{2+}-binding by **1** was indicated to be 1:1 using a Job's plot. The log$K$ for Pb^{2+}-binding by **1**–**3** were determined in CH_3CN/CH_2Cl_2 (1:1) to be 6.63±0.06, 6.20±0.15, and 6.47±0.44, respectively (Figure S18 in the Supporting Information), indicating that the binding is weakest for **2**.

It is pertinent to consider the following to rationalize the emission responses upon addition of Pb^{2+} in Figure 8: a) A blue-shifted emission may be ascribed to 1) disruption of π–π interactions within the (Pt-salphen)$_2$ unit (this would be accompanied by a "monomer-like" structured emission), or/and 2) stabilization of salphen O(p) orbitals, and hence destabilization of O(p)→π*(diimine) transition, upon Pb^{2+} -binding (this is entirely consistent with the observed blue-shift for the lowest-energy absorption band of the binuclear complexes with Pb^{2+}). b) Upon Pb^{2+}-binding, emission enhancement may be afforded by 1) a reduction in intramolecular self-quenching due to weakened or disrupted π–π interactions, or/and 2) rigidification of the molecular framework. c) Pb^{2+} ions can interact with the Pt-salphen luminophore and invariably causes emission quenching.

Therefore, we propose that for **1**, binding of Pb^{2+} within the (Pt-salphen)$_2$ cavity results in blue-shifted "monomer-like" emission, which arises from O(p) stabilization as well as disruption of intramolecular π–π interactions (as indicated by DFT calculations). Consequently, the reduction in self-quenching (and possibly increased host rigidification) would counter-balance the expected Pb^{2+}-mediated emission quenching to afford enhanced (or undiminished) structured emission at λ_{max} 607 nm. Notwithstanding the different coordination cavities formed by the *syn* and *anti* (Pt-salphen)$_2$ unit in **1** and **3** respectively, the DFT calculations revealed comparable Pb^{2+} binding modes and Pb–O(salphen) distances. For **3** however, addition of Pb^{2+} produced a relatively unstructured emission band and a smaller blue-shift (to λ_{max} 616 nm). This implies that intramolecular π–π interactions may persist to some extent (the blue-shift may be predominantly caused by O(p) stabilization upon $Pb^{2+}\cdots$O-(salphen) coordination), and is consistent with the close interplanar separation of 3.39 Å in the calculated structure of $[\mathbf{3}+Pb+ClO_4]^+$. Such a Pb^{2+}-binding mode, in which π–π interactions can prevail and self-quenching is accordingly not reduced, could conceivably afford diminished emission intensity due to Pb^{2+}-mediated quenching, as is observed for **3**. We suggest that a similar rationale to that for **1** can account for the blue-shifted, structured emission observed for **2** with Pb^{2+}, although only a weak π–π interaction is disrupted and the binding is evidently weaker.

To summarize, the evidence herein indicates that a (Pt-salphen)$_2$ cavity displaying intramolecular interactions is required to afford a blue-shifted emission response to Pb^{2+} ions. The following discussion focuses on complex **1**, which gives the strongest Pb^{2+}-binding. Interaction with Pb^{2+} could occur by coordination within the (Pt-salphen)$_2$ cavity, but interaction and quenching with Cu^{2+} (or Hg^{2+}) apparently takes place outside the cavity. The plausibility for O_4-coordination of Pb^{2+} by the O(salphen) groups is suggested by the following: a) the dominant species in the ESI-MS was identified as $[\mathbf{1}+Pb+ClO_4]^+$, which bears a striking resemblance to the X-ray crystal structure of $[\{Ni(salen)\}_2\cdot Ba(ClO_4)_2(thf)]$ featuring two mononuclear Ni(salen) acting as bidentate moieties;[40] b) O-complexation by metal-Schiff base assemblies,[3–5] including the supramolecular aggregation of Zn-salphen complexes to generate gels and nanofibers through Zn$\cdots$O(salphen) interactions,[7] is well-documented; c) in the energy-minimized calculated structure of $[\mathbf{1}+Pb+ClO_4]^+$, the Pb^{2+} ion is coordinated by four O(salphen) donors plus a bidentate perchlorate group. Overall, the photophysical responses and contrasting results for control complexes, together with the above discussion, are consistent with the binding of a perchlorate-coordinated Pb^{2+} ion in the cavity of **1**, which causes conformational changes (including axial rotation) and disrupts the π-stacked interactions within the (Pt-salphen)$_2$ moiety; the original low-energy π-stacked emission is therefore transformed by the Pb^{2+} ion into the blue-shifted "monomer-like" emission of non-interacting Pt-salphen units and self-quenching becomes minimized (although other binding mechanisms cannot be disregarded).

Conclusion

The M^{n+}-binding abilities of rigidly-linked (Pt-salphen)$_2$ hosts, which constitute a new class of axially rotating coordination architectures and may be considered as phosphorescent relatives of 12-crown-4, have been investigated. Differences between the photophysical properties and ion-selective responses of (Pt-salphen)$_2$ complexes anchored to substituted xanthene, dibenzofuran, and biphenylene backbones have been examined and rationalized. It is apparent that the nature of the backbone can dictate the relative topology of the cofacial Pt-salphen moieties, the prevalence of intramolecular π–π interactions, and the dimensions of the potential binding cavity in these frameworks. A plausible mechanism for Pb^{2+}-binding is proposed based on the interplay between O-chelation and perturbation of intramolecular π-contacts within the environmentally responsive (Pt-salphen)$_2$ luminophore, which in turn affects the self-quenching and emission characteristics. These results may carry important implications for luminescent complexes and sensory materials that engage in intramolecular interactions, and which undergo photophysical changes in response to external stimuli and guest-binding. Considering their structural diversity, the development of supramolecular O-coordination by multinuclear metal-Schiff base assemblies is appealing. Studies are continuing to create shape-persistent phosphorescent coordination frameworks that exhibit novel supramolecular behavior and applications.

Experimental Section

General considerations: Solvents for syntheses (analytical grade) were used without further purification and all metalation reactions were performed under a nitrogen atmosphere. Solvents for photophysical measurements were purified according to conventional methods. ^{1}H NMR spectra were obtained on Bruker DRX 300 and 400 FT-NMR spectrometers (ppm) by using Me_4Si as internal standard. ESI mass spectra were measured on a Perkin–Elmer SCIEX API 365 mass spectrometer. IR spectra were recorded on a Perkin–Elmer 1600 series FT-IR spectrophotometer. Elemental analyses were performed on a Vario EL elemental analyzer (Elementar Analysensysteme GmbH). Full experimental and characterization details are provided in the Supporting Information. Complex **5** was synthesized by modification of a literature method.[28a]

UV/Vis absorption spectra were obtained on an Agilent 8453 diode array spectrophotometer. Steady-state emission spectra were recorded on a SPEX FluoroLog 3-TCSPC spectrophotometer equipped with a Hamamatsu R928 PMT detector, and emission lifetime measurements were conducted by using NanoLed sources in the fast MCS mode and checked using the TCSPC mode. Sample and standard solutions were degassed with at least three freeze-pump-thaw cycles. Low-temperature (77 K) emission spectra for glasses and solid-state samples were recorded in 5 mm diameter quartz tubes that were placed in a liquid nitrogen Dewar equipped with quartz windows. The emission quantum yield was measured by using $[Ru(bpy)_3](PF_6)_2$ in degassed acetonitrile as the standard ($\Phi_r = 0.062$) and calculated by: $\Phi_s = \Phi_r(B_r/B_s)(n_s/n_r)^2(D_s/D_r)$, in which the subscripts s and r refer to sample and reference standard solution, respectively, n is the refractive index of the solvents, D is the integrated intensity, and Φ is the luminescence quantum yield. The quantity B is calculated by the equation: $B = 1–10^{-AL}$; in which A is the absorbance at the excitation wavelength and L is the optical path length. Errors for λ (± 1 nm), τ ($\pm 10\,\%$), and Φ ($\pm 10\,\%$) are estimated. Transient absorption spectra at room temperature were recorded using the spectral mode on an Edinburgh Instruments LP920-KS equipped with an ICCD detector. The excitation source for the transient absorption measurement was the third harmonic output (355 nm; 6–8 ns full width at half-maximum (fwhm) pulse width) of a Spectra-Physics Quanta-Ray Q-switched LAB-150 pulsed Nd:YAG laser (10 Hz). Solutions of Pt^{II} complexes and metal perchlorate salts were prepared in CH_3CN (spectroscopic grade). Absorption and emission titrations were carried out in a quartz cuvette by addition of small volumes of metal ion solutions (5×10^{-3} M) to the Pt^{II} complex.

Crystal data were collected on an Oxford Diffraction Gemini S Ultra X-ray single-crystal diffractometer using graphite-monochromated $Cu_{K\alpha}$ radiation ($\lambda = 1.54184$ Å). The structures were solved by direct methods and refined using the SHELXL-97 program on a PC.[43] DFT calculations on molecular structures were performed at the B3LYP level with the CEP-31G basis set using the Gaussian 09 program package.[44] In each case, the energy-minimized calculated structure was confirmed to be a minimum from vibrational frequency calculations.

Synthesis of 3: 3,6-Di-*tert*-butylbiphenylene-1,8-diyldiboronic acid **B3** (66 mg, 0.19 mmol), **L1** (220 mg, 0.38 mmol), $[Pd(PPh_3)_4]$ (44 mg, 0.04 mmol), and K_2CO_3 (78 mg, 0.56 mmol) were charged into a two-necked flask under nitrogen. DMF (20 mL) was degassed by using three freeze-pump-thaw cycles and added, and the mixture was stirred at 75 °C for 7 days. The solvent was removed and the residue was dissolved in CH_2Cl_2 (50 mL). After washing with water (3 × 30 mL), the organic phase was dried over anhydrous Na_2SO_4 and concentrated in vacuo. The crude product was purified by column chromatography (SiO_2, ethyl acetate/hexane = 1:1) to afford a dark red solid (50 mg, 21 %). ^{1}H NMR (CD_2Cl_2, 400 MHz): $\delta = 7.80$ (s, 2H), 7.61 (s, 2H), 7.60–7.51 (m, 6H), 7.32 (d, $J = 8.4$ Hz, 2H), 7.26 (ddd, $J = 14.0$, 8.0, 1.2 Hz, 4H), 7.13 (d, $J = 8.4$ Hz, 2H), 7.04 (d, $J = 1.6$ Hz, 2H), 7.00 (dd, $J = 6.4$, 1.6 Hz, 4H), 6.87 (d, $J = 8.4$ Hz, 2H), 6.80–6.74 (m, 4H), 1.37 ppm (s, 18H); ESI-MS (m/z): 1279.1 $[M+H]^+$; elemental analysis calcd (%) for $C_{60}H_{48}N_4O_4Pt_2$: C 56.34, H 3.78, N 4.38; found C 56.19, H 3.78, N 4.44.

Acknowledgements

The work described in this paper was fully supported by grants from the Research Grants Council of the Hong Kong SAR, China (CityU 100408 and 100212). The flash photolysis system was supported by a Special Equipment Grant from the University Grants Committee of the Hong Kong SAR, China (SEG_CityU02).

---

[1] a) J.-M. Lehn, *Angew. Chem.* **1988**, *100*, 91–116; *Angew. Chem. Int. Ed. Engl.* **1988**, *27*, 89–112; b) K. Hiratani, M. Albrecht, *Chem. Soc. Rev.* **2008**, *37*, 2413–2421; c) M. D. Pluth, R. G. Bergman, K. N. Raymond, *Acc. Chem. Res.* **2009**, *42*, 1650–1659.

[2] a) A. W. Kleij, *Chem. Eur. J.* **2008**, *14*, 10520–10529; b) C. J. Whiteoak, G. Salassa, A. W. Kleij, *Chem. Soc. Rev.* **2012**, *41*, 622–631.

[3] a) A. J. Gallant, M. J. MacLachlan, *Angew. Chem.* **2003**, *115*, 5465–5468; *Angew. Chem. Int. Ed.* **2003**, *42*, 5307–5310; b) J. K.-H. Hui, M. J. MacLachlan, *Chem. Commun.* **2006**, 2480–2482; c) P. D. Frischmann, J. Jiang, J. K.-H. Hui, J. J. Grzybowski, M. J. MacLachlan, *Org. Lett.* **2008**, *10*, 1255–1258; d) S. Guieu, A. K. Crane, M. J. MacLachlan, *Chem. Commun.* **2011**, *47*, 1169–1171.

[4] a) C. T. L. Ma, M. J. MacLachlan, *Angew. Chem.* **2005**, *117*, 4250–4254; *Angew. Chem. Int. Ed.* **2005**, *44*, 4178–4182; b) J. H. Chong, S. Jooya Ardakani, K. J. Smith, M. J. MacLachlan, *Chem. Eur. J.* **2009**, *15*, 11824–11828; c) J. Dömer, J. C. Slootweg, F. Hupka, K. Lammertsma, F. E. Hahn, *Angew. Chem.* **2010**, *122*, 6575–6578; *Angew. Chem. Int. Ed.* **2010**, *49*, 6430–6433; d) P. D. Frischmann, G. A. Facey, P. Y. Ghi, A. J. Gallant, D. L. Bryce, F. Lelj, M. J. MacLachlan, *J. Am. Chem. Soc.* **2010**, *132*, 3893–3908; e) M. V. Escárcega-Bobadilla, G. Salassa, M. Martínez Belmonte, E. C. Escudero-Adán, A. W. Kleij, *Chem. Eur. J.* **2012**, *18*, 6805–6810.

[5] a) M. Cametti, M. Nissinen, A. Dalla Cort, L. Mandolini, K. Rissanen, *J. Am. Chem. Soc.* **2005**, *127*, 3831–3837; b) S. Akine, T. Taniguchi, T. Nabeshima, *J. Am. Chem. Soc.* **2006**, *128*, 15765–15774; c) E. R. Libra, M. J. Scott, *Chem. Commun.* **2006**, 1485–1487; d) C.-T. Chen, Y.-H. Lin, T.-S. Kuo, *J. Am. Chem. Soc.* **2008**, *130*, 12842–12843.

[6] a) M. Martínez Belmonte, S. J. Wezenberg, R. M. Haak, D. Anselmo, E. C. Escudero-Adán, J. Benet-Buchholz, A. W. Kleij, *Dalton Trans.* **2010**, *39*, 4541–4550; b) J. A. A. W. Elemans, S. J. Wezenberg, M. J. J. Coenen, E. C. Escudero-Adán, J. Benet-Buchholz, D. den

Boer, S. Speller, A. W. Kleij, S. De Feyter, *Chem. Commun.* **2010**, *46*, 2548–2550.

[7] a) J. K.-H. Hui, Z. Yu, T. Mirfakhrai, M. J. MacLachlan, *Chem. Eur. J.* **2009**, *15*, 13456–13465; b) J. K.-H. Hui, P. D. Frischmann, C.-H. Tso, C. A. Michal, M. J. MacLachlan, *Chem. Eur. J.* **2010**, *16*, 2453–2460; c) P. D. Frischmann, S. Guieu, R. Tabeshi, M. J. MacLachlan, *J. Am. Chem. Soc.* **2010**, *132*, 7668–7675.

[8] A. C. W. Leung, M. J. MacLachlan, *J. Mater. Chem.* **2007**, *17*, 1923–1932.

[9] a) G. Li, W. Yu, J. Ni, T. Liu, Y. Liu, E. Sheng, Y. Cui, *Angew. Chem.* **2008**, *120*, 1265–1269; *Angew. Chem. Int. Ed.* **2008**, *47*, 1245–1249; b) S. J. Wezenberg, G. Salassa, E. C. Escudero-Adán, J. Benet-Buchholz, A. W. Kleij, *Angew. Chem.* **2011**, *123*, 739–742; *Angew. Chem. Int. Ed.* **2011**, *50*, 713–716.

[10] a) S.-Y. Liu, D. G. Nocera, *J. Am. Chem. Soc.* **2005**, *127*, 5278–5279; b) J. Y. Yang, D. G. Nocera, *J. Am. Chem. Soc.* **2007**, *129*, 8192–8198.

[11] a) F. H. Zelder, J. Rebek Jr., *Chem. Commun.* **2006**, 753–754; b) M. Shibasaki, M. Kanai, S. Matsunaga, N. Kumagai, *Acc. Chem. Res.* **2009**, *42*, 1117–1127; c) M. Taherimehr, A. Decortes, S. M. Al-Amsyar, W. Lueangchaichaweng, C. J. Whiteoak, E. C. Escudero-Adán, A. W. Kleij, P. P. Pescarmona, *Catal. Sci. Technol.* **2012**, *2*, 2231–2237.

[12] a) K. E. Splan, A. M. Massari, G. A. Morris, S.-S. Sun, E. Reina, S. T. Nguyen, J. T. Hupp, *Eur. J. Inorg. Chem.* **2003**, 2348–2351; b) H. Houjou, M. Ito, K. Araki, *Inorg. Chem.* **2009**, *48*, 10703–10707.

[13] a) A. C. W. Leung, J. K.-H. Hui, J. H. Chong, M. J. MacLachlan, *Dalton Trans.* **2009**, 5199–5210; b) T. J. Dunn, C. F. Ramogida, C. Simmonds, A. Paterson, E. W. Y. Wong, L. Chiang, Y. Shimazaki, T. Storr, *Inorg. Chem.* **2011**, *50*, 6746–6755; c) T. J. Dunn, L. Chiang, C. F. Ramogida, M. I. Webb, D. Savard, M. Sakaguchi, T. Ogura, Y. Shimazaki, T. Storr, *Dalton Trans.* **2012**, *41*, 7905–7914.

[14] N. Komiya, T. Muraoka, M. Iida, M. Miyanaga, K. Takahashi, T. Naota, *J. Am. Chem. Soc.* **2011**, *133*, 16054–16061.

[15] a) R. G. Konsler, J. Karl, E. N. Jacobsen, *J. Am. Chem. Soc.* **1998**, *120*, 10780–10781; b) H. J. Yoon, C. A. Mirkin, *J. Am. Chem. Soc.* **2008**, *130*, 11590–11591; c) B. A. Rodriguez, M. Delferro, T. J. Marks, *J. Am. Chem. Soc.* **2009**, *131*, 5902–5919; d) S. I. Vagin, R. Reichardt, S. Klaus, B. Rieger, *J. Am. Chem. Soc.* **2010**, *132*, 14367–14369; e) K. Nakano, S. Hashimoto, K. Nozaki, *Chem. Sci.* **2010**, *1*, 369–373; f) P. C. B. Widger, S. M. Ahmed, G. W. Coates, *Macromolecules* **2011**, *44*, 5666–5670.

[16] K. Rurack, U. Resch-Genger, *Chem. Soc. Rev.* **2002**, *31*, 116–127.

[17] a) J. P. Collman, P. S. Wagenknecht, J. E. Hutchison, *Angew. Chem.* **1994**, *106*, 1620–1639; *Angew. Chem. Int. Ed. Engl.* **1994**, *33*, 1537–1554; b) J. S. Nowick, P. Ballester, F. Ebmeyer, J. Rebek, Jr., *J. Am. Chem. Soc.* **1990**, *112*, 8902–8906; c) E. Benaksas Schwartz, C. B. Knobler, D. J. Cram, *J. Am. Chem. Soc.* **1992**, *114*, 10775–10784; d) Y. Hong, J. W. Y. Lam, B. Z. Tang, *Chem. Commun.* **2009**, 4332–4353.

[18] a) T. Nakano, T. Yade, *J. Am. Chem. Soc.* **2003**, *125*, 15474–15484; b) T.-Q. Nguyen, R. Martel, P. Avouris, M. L. Bushey, L. Brus, C. Nuckolls, *J. Am. Chem. Soc.* **2004**, *126*, 5234–5242; c) M. M. Elmahdy, X. Dou, M. Mondeshki, G. Floudas, H.-J. Butt, H. W. Spiess, K. Müllen, *J. Am. Chem. Soc.* **2008**, *130*, 5311–5319; d) J. He, J. L. Crase, S. H. Wadumethrige, K. Thakur, L. Dai, S. Zou, R. Rathore, C. S. Hartley, *J. Am. Chem. Soc.* **2010**, *132*, 13848–13857; e) E. Ohta, H. Sato, S. Ando, A. Kosaka, T. Fukushima, D. Hashizume, M. Yamasaki, K. Hasegawa, A. Muraoka, H. Ushiyama, K. Yamashita, T. Aida, *Nat. Chem.* **2011**, *3*, 68–73.

[19] a) J. Rosenthal, T. D. Luckett, J. M. Hodgkiss, D. G. Nocera, *J. Am. Chem. Soc.* **2006**, *128*, 6546–6547; b) C. H. Lee, D. K. Dogutan, D. G. Nocera, *J. Am. Chem. Soc.* **2011**, *133*, 8775–8777; c) D. K. Dogutan, R. McGuire, Jr., D. G. Nocera, *J. Am. Chem. Soc.* **2011**, *133*, 9178–9180.

[20] a) F. Cozzi, F. Ponzini, R. Annunziata, M. Cinquini, J. S. Siegel, *Angew. Chem.* **1995**, *107*, 1092–1094; *Angew. Chem. Int. Ed. Engl.* **1995**, *34*, 1019–1020; b) T. Mizuno, W.-H. Wei, L. R. Eller, J. L. Sessler, *J. Am. Chem. Soc.* **2002**, *124*, 1134–1135; c) V. J. Chebny, R. Rathore, *J. Am. Chem. Soc.* **2007**, *129*, 8458–8465; d) S. Dutta, D.-K. Bučar, L. R. MacGillivray, *Org. Lett.* **2011**, *13*, 2260–2262; e) D. P. Iwaniuk, C. Wolf, *J. Am. Chem. Soc.* **2011**, *133*, 2414–2417.

[21] a) S. A. McFarland, N. S. Finney, *J. Am. Chem. Soc.* **2001**, *123*, 1260–1261; b) S. A. McFarland, N. S. Finney, *J. Am. Chem. Soc.* **2002**, *124*, 1178–1179; c) M. Barboiu, L. Prodi, M. Montalti, N. Zaccheroni, N. Kyritsakas, J.-M. Lehn, *Chem. Eur. J.* **2004**, *10*, 2953–2959; d) J. V. Mello, N. S. Finney, *J. Am. Chem. Soc.* **2005**, *127*, 10124–10125; e) C. Wolf, S. Liu, B. C. Reinhardt, *Chem. Commun.* **2006**, 4242–4244.

[22] C. W. Chen, H. W. Whitlock, Jr., *J. Am. Chem. Soc.* **1978**, *100*, 4921–4922.

[23] a) F.-G. Klärner, B. Kahlert, *Acc. Chem. Res.* **2003**, *36*, 919–932; b) A. J. Goshe, I. M. Steele, B. Bosnich, *J. Am. Chem. Soc.* **2003**, *125*, 444–451; c) N. C. Gianneschi, S.-H. Cho, S. T. Nguyen, C. A. Mirkin, *Angew. Chem.* **2004**, *116*, 5619–5623; *Angew. Chem. Int. Ed.* **2004**, *43*, 5503–5507; d) S. Ulrich, J.-M. Lehn, *Chem. Eur. J.* **2009**, *15*, 5640–5645; e) H. Yoo, J. Yang, A. Yousef, M. R. Wasielewski, D. Kim, *J. Am. Chem. Soc.* **2010**, *132*, 3939–3944; f) I. Pochorovski, M.-O. Ebert, J.-P. Gisselbrecht, C. Boudon, W. B. Schweizer, F. Diederich, *J. Am. Chem. Soc.* **2012**, *134*, 14702–14705.

[24] a) W.-L. Tong, M. C. W. Chan, N. Zhu, S.-K. Leung, *Dalton Trans.* **2009**, 4741–4746; b) W.-L. Tong, M. C. W. Chan, S.-M. Yiu, *Organometallics* **2010**, *29*, 6377–6383.

[25] Z. Guo, M. C. W. Chan, *Chem. Eur. J.* **2009**, *15*, 12585–12588.

[26] S. Sun, W.-L. Tong, M. C. W. Chan, *Macromol. Rapid Commun.* **2010**, *31*, 1965–1969.

[27] a) S.-W. Lai, M. C. W. Chan, T.-C. Cheung, S.-M. Peng, C.-M. Che, *Inorg. Chem.* **1999**, *38*, 4046–4055; b) K.-H. Wong, M. C. W. Chan, C.-M. Che, *Chem. Eur. J.* **1999**, *5*, 2845–2849; c) P. Wu, D.-L. Ma, C.-H. Leung, S.-C. Yan, N. Zhu, R. Abagyan, C.-M. Che, *Chem. Eur. J.* **2009**, *15*, 13008–13021.

[28] a) Y.-Y. Lin, S.-C. Chan, M. C. W. Chan, Y.-J. Hou, N. Zhu, C.-M. Che, Y. Liu, Y. Wang, *Chem. Eur. J.* **2003**, *9*, 1263–1272; b) C.-M. Che, S.-C. Chan, H.-F. Xiang, M. C. W. Chan, Y. Liu, Y. Wang, *Chem. Commun.* **2004**, 1484–1485; c) C.-M. Che, C.-C. Kwok, S.-W. Lai, A. F. Rausch, W. J. Finkenzeller, N. Zhu, H. Yersin, *Chem. Eur. J.* **2010**, *16*, 233–247.

[29] W. Wu, J. Sun, S. Ji, W. Wu, J. Zhao, H. Guo, *Dalton Trans.* **2011**, *40*, 11550–11561.

[30] Z. Guo, W.-L. Tong, M. C. W. Chan, *Chem. Commun.* **2009**, 6189–6191.

[31] A. Rajca, A. Safronov, S. Rajca, C. R. Ross II, J. J. Stezowski, *J. Am. Chem. Soc.* **1996**, *118*, 7272–7279.

[32] S. M. H. Kabir, M. Hasegawa, Y. Kuwatani, M. Yoshida, H. Matsuyama, M. Iyoda, *J. Chem. Soc. Perkin Trans. 1* **2001**, 159–165.

[33] Crystal data for **1**: $C_{63}H_{54}N_4O_5Pt_2$, $M_r=1337.28$, monoclinic, $P2_1/c$, $a=15.8344(5)$, $b=27.2295(9)$, $c=11.5818(4)$ Å, $\beta=101.982(3)°$, $V=4884.9(3)$ Å^3, $Z=4$, $T=133(2)$ K, $\rho_{\text{cald}}=1.818\,\text{g}\,\text{cm}^{-3}$, $m(\text{Cu}_{\text{K}\alpha})=11.031\,\text{mm}^{-1}$, $F(000)=2624$, $2\theta_{\max}=134.0°$; 8697 independent reflections ($R_{\text{int}}=0.023$), 675 variable parameters, $R_1=0.0300$ $[I>2\sigma(I)]$, $wR_2=0.0797$. Crystal data for **3**: $C_{60}H_{48}N_4O_4Pt_2\cdot H_2O\cdot$(ethyl acetate), $M_r=1385.32$, monoclinic, $P2_1/n$, $a=18.1544(2)$, $b=13.87693(16)$, $c=22.4224(3)$ Å, $\beta=109.5358(14)°$, $V=5323.63(11)$ Å^3, $Z=4$, $T=133(2)$ K, $\rho_{\text{cald}}=1.728\,\text{g}\,\text{cm}^{-3}$, $m(\text{Cu}_{\text{K}\alpha})=10.174\,\text{mm}^{-1}$, $F(000)=2728$, $2\theta_{\max}=134.0°$; 9490 independent reflections ($R_{\text{int}}=0.021$), 702 variable parameters, $R_1=0.0237$ $[I>2\sigma(I)]$, $wR_2=0.0633$. CCDC-921758 (**1**) and 921759 (**3**) contain the supplementary crystallographic data for this paper. These data can be obtained free of charge from The Cambridge Crystallographic Data Centre via www.ccdc.cam.ac.uk/data_request/cif.

[34] a) V. M. Miskowski, V. H. Houlding, *Inorg. Chem.* **1991**, *30*, 4446–4452; b) J. A. Bailey, M. G. Hill, R. E. Marsh, V. M. Miskowski, W. P. Schaefer, H. B. Gray, *Inorg. Chem.* **1995**, *34*, 4591–4599; c) T. J. Wadas, Q.-M. Wang, Y.-J. Kim, C. Flaschenreim, T. N. Blanton, R. Eisenberg, *J. Am. Chem. Soc.* **2004**, *126*, 16841–16849; d) W. Lu, M. C. W. Chan, N. Zhu, C.-M. Che, C. Li, Z. Hui, *J. Am. Chem. Soc.* **2004**, *126*, 7639–7651.

[35] S. D. Cummings, R. Eisenberg, *J. Am. Chem. Soc.* **1996**, *118*, 1949–1960.

[36] W. Lu, M. C. W. Chan, K.-K. Cheung, C.-M. Che, *Organometallics* **2001**, *20*, 2477–2486.

[37] a) Y. Shen, B. P. Sullivan, *Inorg. Chem.* **1995**, *34*, 6235–6236; b) M.-J. Li, C.-C. Ko, G.-P. Duan, N. Zhu, V. W.-W. Yam, *Organometallics* **2007**, *26*, 6091–6098; c) M.-L. Ho, Y.-M. Cheng, L.-C. Wu, P.-T. Chou, G.-H. Lee, F.-C. Hsu, Y. Chi, *Polyhedron* **2007**, *26*, 4886–4892.

[38] The expected blue-shift (to λ_{max} 605 nm) for the 639 nm emission in CH_3CN was obtained upon addition of 3.0 equiv of Pb^{2+}. Subsequent addition of TMEDA (9.0 equiv), acting as Pb^{2+} scavenger, caused the emission spectrum and lifetime to revert back to the original.

[39] At a declustering potential of 50 V, the 1:1 $[\mathbf{3}+Pb]^{2+}$ species at m/z 742.8, with 0.5 amu peak separations, is dominant. Cooperative 2:2 binding, which would afford 0.25 amu separations, can therefore be discounted (furthermore, non-sigmoidal binding curve gives excellent fit for 1:1 binding, and the Hill plot does not show positive cooperation).

[40] L. Carbonaro, M. Isola, P. La Pegna, L. Senatore, F. Marchetti, *Inorg. Chem.* **1999**, *38*, 5519–5525.

[41] J. R. Berenguer, A. Díez, J. Fernández, J. Forniés, A. García, B. Gil, E. Lalinde, M. T. Moreno, *Inorg. Chem.* **2008**, *47*, 7703–7716.

[42] A. L. Balch, V. J. Catalano, M. A. Chatfield, J. K. Nagle, M. M. Olmstead, P. E. Reedy, Jr., *J. Am. Chem. Soc.* **1991**, *113*, 1252–1258.

[43] G. M. Sheldrick, SHELXS-97 and SHELXL-97, Programs for Crystal Structure Solution and Refinement, University of Göttingen, Göttingen, Germany, **1997**.

[44] Gaussian 09, Revision B.1, M. J. Frisch, G. W. Trucks, H. B. Schlegel, G. E. Scuseria, M. A. Robb, J. R. Cheeseman, G. Scalmani, V. Barone, B. Mennucci, G. A. Petersson, H. Nakatsuji, M. Caricato, X. Li, H. P. Hratchian, A. F. Izmaylov, J. Bloino, G. Zheng, J. L. Sonnenberg, M. Hada, M. Ehara, K. Toyota, R. Fukuda, J. Hasegawa, M. Ishida, T. Nakajima, Y. Honda, O. Kitao, H. Nakai, T. Vreven, J. A. Montgomery, Jr., J. E. Peralta, F. Ogliaro, M. Bearpark, J. J. Heyd, E. Brothers, K. N. Kudin, V. N. Staroverov, R. Kobayashi, J. Normand, K. Raghavachari, A. Rendell, J. C. Burant, S. S. Iyengar, J. Tomasi, M. Cossi, N. Rega, N. J. Millam, M. Klene, J. E. Knox, J. B. Cross, V. Bakken, C. Adamo, J. Jaramillo, R. Gomperts, R. E. Stratmann, O. Yazyev, A. J. Austin, R. Cammi, C. Pomelli, J. W. Ochterski, R. L. Martin, K. Morokuma, V. G. Zakrzewski, G. A. Voth, P. Salvador, J. J. Dannenberg, S. Dapprich, A. D. Daniels, Ö. Farkas, J. B. Foresman, J. V. Ortiz, J. Cioslowski, D. J. Fox, Gaussian, Inc., Wallingford CT, USA, **2009**.

Received: February 2, 2013

Supramolecular Chemistry

*Z. Guo, S.-M. Yiu, M. C. W. Chan** .... ▮▮▮▮–▮▮▮▮

Shape-Persistent (Pt-salphen)$_2$ Phosphorescent Coordination Frameworks: Structural Insights and Selective Perturbations

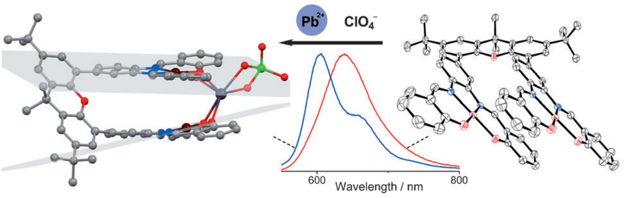

To π or not to π? The ratiometric phosphorescent ion-selective responses of axially rotating binuclear assemblies have been investigated by using X-ray crystallography, DFT calculations, and various spectroscopic techniques to provide an insight into the binding mechanism (see figure). These results may carry important implications for stimuli-responsive luminescent host complexes that engage in intramolecular interactions.